CrossMark

Complex nonlinearities of rogue waves in generalized inhomogeneous higher-order nonlinear Schrödinger equation

N. Song · W. Zhang · M. H. Yao

Abstract In this paper, the Nth-order rogue waves are investigated for an inhomogeneous higher-order nonlinear Schrödinger equation. Based on the Heisenberg ferromagnetic spin system, the higher-order nonlinear Schrödinger equation is generated. The generalized Darboux transformation is constructed by the Darboux matrix. The solutions of the Nth-order rogue waves are given in terms of a recursive formula. There are complex nonlinear phenomena in the rogue waves, add the first-order to the fourth-order rogue waves are discussed in some figures obtained by analytical solutions. It is shown that the general Nth-order rogue waves contain $2n - 1$ free parameters. The free parameters play a crucial role to affect the dynamic distributions of the rogue waves. The results obtained in this paper will be useful to understand the generation mechanism of the rogue wave.

Keywords Rogue wave · Higher-order nonlinear Schrödinger equation · Darboux transformation · Complex nonlinearities

N. Song · W. Zhang (✉) · M. H. Yao
College of Mechanical Engineering, Beijing University
of Technology, Beijing 100022,
People's Republic of China
e-mail: sandyzhang0@yahoo.com

N. Song
Department of Mathematics, North University of China,
Taiyuan 030051, Shanxi, People's Republic of China
e-mail: songni@emails.bjut.edu.cn

1 Introduction

The rogue wave is the giant single wave, which was firstly found in the ocean [1]. The single rogue wave is referred to the fundamental form of the hierarchy for the rogue wave. The amplitude of the rogue wave is two to three times higher than those of the surrounding waves. One of the features of the rogue wave is that it appears from nowhere and disappears without a trace [2]. In the nature, the rogue wave is very dangerous, which can appear unexpectedly and forms the larger amplitude in 1 min to shred a boat. Beyond oceanic expanses, the rogue wave has also been found experimentally in optical fibers [3], Bose–Einstein condensates (BECs) [4], superfluids [5] and so on. In a word, the rogue waves have the characteristic of the burst, the localization, the short time and the dramatic concentration of the energy. The phenomenon in the rogue waves has nonlinear characteristic. Thus, the linear wave theories based on the superposition principle are not used to explain the complex phenomenon of the rogue wave in the ocean, the optical fibers and the engineering field. The nonlinear theories [6–8] are being applied to analyze these nonlinear phenomena of the rogue waves. The rogue wave has been an important issue in the fields of the nonlinear science.

One of the important known models for the rogue wave is the nonlinear Schrödinger (NLS) equation. Many research results have been obtained for the NLS equation. For example, the first-order rational solutions [9,10], the control of the rogue waves [11], the soliton

solutions [12] and Darboux transformation (DT) [13] of the NLS equation are studied in detail. Apart from the NLS equation, researchers have also investigated the solution of the rogue wave for the generalized nonlinear Schrödinger (GNLS) equation [14], (3+1)-dimensional GNLS equation [15], the higher-order NLS equation [16], the dissipative NLS equation with a variable coefficient [17], the two-component NLS equations [18] and the general two-coupled NLS equation [19].

The stability of solutions is also an important problem for waves. There are a few achievements of this aspect; for example, Dai et al. [20,21] investigated the stability of analytical spatial soliton solutions for a two-dimensional NLS equation with power-law nonlinearity in PT-symmetric potentials. They used the linear stability theory and the direct numerical simulations to analyze the stability of the solutions.

Motivated by the aforementioned works, in this paper, an inhomogeneous higher-order NLS equation is considered as follows [22]

$$
i\frac{\partial q}{\partial t} + \varepsilon\frac{\partial^4 q}{\partial x^4} + 8\varepsilon |q|^2 \frac{\partial^2 q}{\partial x^2} + 2\varepsilon q^2 \frac{\partial^2 q^*}{\partial x^2}
$$
$$
+ 4\varepsilon \left|\frac{\partial q}{\partial x}\right|^2 q + 6\varepsilon q^* \left(\frac{\partial^2 q}{\partial x^2}\right)^2 + 6\varepsilon |q|^4 q + \frac{\partial^2(fq)}{\partial x^2}
$$
$$
+ 2q\left[f|q|^2 + \int_{-\infty}^{x} \frac{\partial f}{\partial s} |q(s,t)|^2 \,\mathrm{d}s \right] - i\frac{\partial(hq)}{\partial x} = 0,
$$
$$(1)$$

where $q(x,t)$ is a complex function, t and x denote the scaled time and spatial coordinate, respectively, f and h represent the inhomogeneousness present in the medium and are the linear functions of spatial variable x, which are of the form

$$
f = f_1 x + f_2, \quad h = h_1 x + h_2, \tag{2}
$$

f_j and $h_j (j = 1, 2)$ are real constants, ε is a perturbation parameter, and the asterisk represents the complex conjugation.

Equation (1) is generated by deforming the inhomogeneous Heisenberg ferromagnetic spin system with the prolongation structure [22] and the space curve formalism, which describes the dynamics of a site-dependent Heisenberg ferromagnetic spin chain in the highly idealized physical situations. In fact, we also take into account the inhomogeneity or nonuniformity of the realistic physical medium [23,24] in Eq. (1). The inhomogeneous equation has a wide range of applications in the propagation of radio waves in the ionosphere, waves in the ocean, optical pulses in glass fibers, laser radiations in plasma and impurities in magnetic systems [25,26].

Radha [22] used the gauge transformation to construct the multi-solitary solutions of Eq. (1) and discussed the interaction of the soliton. On the basis of the associated linear eigenvalue problems, Zhong et al. [27] gave the bright soliton solutions of Eq. (1) using the prolongation structure theory. However, to the best of our knowledge, there are no reports about the solution of the rogue wave related to Eq. (1), and the construction of the higher-order NLS equation is regarded as a challenging work.

The aim of this paper is to construct the Nth-order solutions of the rogue wave for Eq. (1) using the generalized Darboux transformation, which is an effective approach to derive the solution of the rogue wave [28]. Based on the DT matrix, the generalized Darboux transformation is obtained and the formula for generating the Nth-order solutions of the rogue wave is given.

2 Generalized Darboux transformation for Eq. (1)

Equation (1) is the compatibility condition of the linear spectral problems [22]

$$
\Phi_x = U\Phi = \begin{pmatrix} -i\lambda & q \\ -q^* & i\lambda \end{pmatrix}\Phi, \tag{3a}
$$

$$
\Phi_t = V\Phi = \begin{pmatrix} A & B \\ -B^* & -A \end{pmatrix}\Phi, \tag{3b}
$$

with

$$
A = i\varepsilon\left(q\frac{\partial^2 q^*}{\partial x^2} + q^*\frac{\partial^2 q}{\partial x^2} - \left|\frac{\partial q}{\partial x}\right|^2 \right)
$$
$$
+ 3i\varepsilon |q|^4 - 2\lambda\varepsilon\left(q^*\frac{\partial q}{\partial x} - q\frac{\partial q^*}{\partial x} \right)
$$
$$
- 4i\lambda^2\varepsilon |q|^2 + 8i\varepsilon\lambda^4
$$
$$
+ if|q|^2 + \int_{-\infty}^{x} \frac{\partial f}{\partial s} |q(s,t)|^2 \,\mathrm{d}s
$$
$$
- 2if\lambda^2 - ih\lambda, \tag{4}
$$

$$
B = i\varepsilon\frac{\partial^3 q}{\partial x^3} + 2\varepsilon\lambda\frac{\partial^2 q}{\partial x^2} + 6i\varepsilon |q|^2 \frac{\partial q}{\partial x}
$$
$$
- 4i\varepsilon\lambda^2\frac{\partial q}{\partial x} + 4\varepsilon\lambda |q|^2 q - 8\varepsilon\lambda^3 q
$$
$$
+ i\frac{\partial^2(fq)}{\partial x^2} + 2f\lambda q + hq, \tag{5}
$$

where $\Phi = (\varphi, \phi)^{\mathrm{T}}$ is the vector eigenfunction of the Lax pair (3a) and (3b), q is a potential function, and λ is a constant spectral parameter.

It is easy to verify that the zero-curvature equation

$$U_t - V_x + [U, V] = 0 \tag{6}$$

gives rise to Eq. (1).

The Darboux matrix T is defined as [22]

$$T = \lambda I - S, \quad S = H\Lambda H^{-1}, \tag{7}$$

where

$$I = \begin{pmatrix} 1 & 0 \\ 0 & 1 \end{pmatrix}, \quad H = \begin{pmatrix} \varphi_1 & \phi_1^* \\ \phi_1 & -\varphi_1^* \end{pmatrix}, \quad \Lambda = \begin{pmatrix} \lambda_1 & 0 \\ 0 & \lambda_1^* \end{pmatrix}. \tag{8}$$

Let $\Phi_1 = (\varphi_1, \phi_1)^{\mathrm{T}}$ be an eigenfunction of the Lax pair (3a) and (3b) with a seeding solution $q = q[0]$ and $\lambda = \lambda_1$. It is seen that $(\phi_1^*, -\varphi_1^*)^{\mathrm{T}}$ also satisfies equation (3) with $\lambda = \lambda_1^*$. Choosing different eigenfunctions $\Phi_k = (\varphi_k, \phi_k)^{\mathrm{T}}$ at λ_k, respectively, the aforementioned DT procedure can be easily iterated.

Based on the Darboux matrix T of Eq. (7), the elementary DT of Eq. (1) is given as

$$\Phi_1[0] = T[0]\Phi_1, q[1] = q[0]$$
$$- 2i(\lambda_1 - \lambda_1^*)\frac{\varphi_1[0]\phi_1^*[0]}{|\varphi_1[0]|^2 + |\phi_1[0]|^2}, \tag{9}$$

where

$$T[1] = \lambda_2 I - H[0]\Lambda[1]H[0]^{-1}, \tag{10a}$$

$$T[0] = I, H[0] = \begin{pmatrix} \varphi_1[0] & \phi_1^*[0] \\ \phi_1[0] & -\varphi_1^*[0] \end{pmatrix},$$

$$\Lambda[1] = \begin{pmatrix} \lambda_1 & 0 \\ 0 & \lambda_1^* \end{pmatrix}, \tag{10b}$$

$$\Phi_1[0] = (\varphi_1[0], \phi_1[0])^{\mathrm{T}}$$
$$= (\varphi_1, \phi_1)^{\mathrm{T}} = \Phi_1, q[0] = q. \tag{10c}$$

If N different basic solutions $\Phi_k = (\varphi_k, \phi_k)^{\mathrm{T}} (k = 1, 2, \ldots, N)$ of the Lax pair (3a) and (3b) at $\lambda = \lambda_k (k = 1, 2, \ldots, N)$ are given, the elementary DT is repeated N times. Then, the Nth-step DT of Eq. (1) is

$$\Phi_N[N-1] = T[N-1]T[N-2]\cdots T[1]T[0]\Phi_N, \tag{11a}$$

$$q[N] = q[0] - 2i \sum_{k=1}^{N} (\lambda_1 - \lambda_1^*)$$
$$\times \frac{\varphi_k[k-1]\phi_k^*[k-1]}{|\varphi_k[k-1]|^2 + |\phi_k[k-1]|^2}, \tag{11b}$$

where

$$T[k] = \lambda_{k+1} I - H[k-1]\Lambda[k]H[k-1]^{-1}, \tag{12a}$$

$$H[k-1] = \begin{pmatrix} \varphi_k[k-1] & \phi_k^*[k-1] \\ \phi_k[k-1] & -\varphi_k^*[k-1] \end{pmatrix},$$

$$\Lambda[k] = \begin{pmatrix} \lambda_k & 0 \\ 0 & \lambda_k^* \end{pmatrix}, \tag{12b}$$

$$\Phi_k[k-1] = (T[k-1]T[k-2]\cdots T[1]T[0])|_{\lambda=\lambda_k}$$
$$\Phi_k, (k = 1, 2, \ldots, N). \tag{12c}$$

The initial value is $\Phi_1[0] = (\varphi_1[0], \phi_1[0])^{\mathrm{T}} = (\varphi_1, \phi_1)^{\mathrm{T}} = \Phi_1$. Based on the aforementioned elementary DT, a generalized DT is obtained for Eq. (1). We assume that

$$\Psi = \Phi_1(\lambda_1, \eta) \tag{13}$$

is a special solution of the Lax pair (3a) and (3b), and η is a small parameter.

With the aid of the Taylor series, Ψ can be expanded at $\eta = 0$

$$\Psi = \Phi_1^{[0]} + \Phi_1^{[1]}\eta + \Phi_1^{[2]}\eta^2 + \cdots$$
$$+ \Phi_1^{[m]}\eta^m + o(\eta^m), \tag{14}$$

where $\Phi_1^{[j]} = \frac{1}{j!}\frac{\partial^j}{\partial\lambda^j}\Phi_1(\lambda)|_{\lambda=\lambda_1}$ $(j = 1, 2, \ldots, m)$.

From the above assumption, it is easily found that $\Phi_1^{[0]} = \Phi_1[0]$ is a particular solution of the Lax pair (3a) and (3b) with $q = q[0]$ and $\lambda = \lambda_1$. Therefore, the Nth-step generalized DT is constructed as follows

$$\Phi_1[N-1]$$
$$= \Phi_1^{[0]} + \left[\sum_{l=1}^{N-1} T_1[l]\right]\Phi_1^{[1]}$$
$$+ \left[\sum_{l=1}^{N-1}\sum_{k>l}^{N-1} T_1[k]T_1[l]\right]\Phi_1^{[2]} + \cdots$$
$$+ [T_1[N-1]T_1[N-2]\cdots T_1[1]]\Phi_1^{[N-1]}, \tag{15}$$

$$q[N] = q[N-1]$$
$$- 2i(\lambda_1 - \lambda_1^*)\frac{\varphi_1[N-1]\phi_1[N-1]^*}{|\varphi_1[N-1]|^2 + |\phi_1[N-1]|^2}, \tag{16}$$

where

$$T_1[k] = \lambda_1 I - H_1[k-1]\Lambda[1]H_1[k-1]^{-1}, \tag{17a}$$

$$H_1[k-1] = \begin{pmatrix} \varphi_k[k-1] & \phi_k^*[k-1] \\ \phi_k[k-1] & -\varphi_k^*[k-1] \end{pmatrix}, \tag{17b}$$

$$\Phi_1[k-1] = \begin{pmatrix} \varphi_k[k-1] \\ \phi_k[k-1] \end{pmatrix}, (k = 1, 2, \ldots, N). \tag{17c}$$

Equations (15)–(17) are the recursive formulae of the Nth-step generalized DT for Eq. (1), which can be converted into the $2n \times 2n$ determinant representation using the Crum theorem [29,30]. The recursive formulae are easily used to construct the higher-order solutions of the rogue wave. Based on these solutions of Eq. (1), some figures of interesting higher-order rogue waves will be obtained in the next section.

3 Solutions of rogue waves

For simplicity, the solutions of the rogue waves are calculated when the inhomogeneous parameters are independent of x, namely $f_1 = h_1 = 0$. We choose the parameters $f_2 = \frac{1}{2}$ and $h_2 = \frac{1}{4}$.

We take a periodic plane seed solution $q[0] = a\mathrm{e}^{i\theta}$ with $\theta = kx + \omega t$. Here, a and k are both real constants, and the frequency ω satisfies the nonlinear dispersion relation

$$\omega = k^4\varepsilon - k^2(12\varepsilon a^2 + f) + hk + 2fa^2 + 6\varepsilon a^4. \tag{18}$$

Using the Maple program, the corresponding solution of the linear spectral problem at $\lambda = \frac{k}{2} - ia + \eta^2$ is obtained

$$\Phi_1(\eta) = \begin{pmatrix} (C_1\mathrm{e}^{\rho} + C_2\mathrm{e}^{-\rho})\mathrm{e}^{\frac{i\theta}{2}} \\ (C_2\mathrm{e}^{\rho} + C_1\mathrm{e}^{-\rho})\mathrm{e}^{-\frac{i\theta}{2}} \end{pmatrix}, \tag{19}$$

where

$$C_1 = \sqrt{-\mu + \frac{i}{2}k + i\lambda}, \ C_2$$
$$= \sqrt{\mu + \frac{i}{2}k + i\lambda}, \ \rho = \mu(x + \delta t + \Omega(\eta)), \tag{20a}$$

$$\mu = \sqrt{k\lambda - \frac{k^2}{4} - \lambda^2 - a^2}, \ \Omega(\eta)$$
$$= \sum_{j=1}^{N} (a_j + ib_j)\eta^{2j} \ (a_j, b_j \in R), \tag{20b}$$

$$\delta = \varepsilon k^3 - 2\varepsilon\lambda k^2 - 6\varepsilon ka^2 + 4\varepsilon k\lambda^2$$
$$+ 4\varepsilon\lambda a^2 - 8\varepsilon\lambda^3 - fk + 2f\lambda + h, \tag{20c}$$

where $\Omega(\eta)$ is a separating function and a_j, b_j are real constants.

Letting $\lambda = \frac{k}{2} - ia + \eta^2$ and expanding the vector function $\Phi_1(\eta)$ at $\eta = 0$, we have

$$\Phi_1(\eta) = \Phi_1^{[0]} + \Phi_1^{[1]}\eta^2 + \Phi_1^{[2]}\eta^4 + \Phi_1^{[3]}\eta^6$$
$$+ \Phi_1^{[4]}\eta^8 \ldots + \Phi_1^{[m]}\eta^{2m} + \cdots, \tag{21}$$

with

$$\Phi_1^{[0]} = \begin{pmatrix} \varphi_1^{[0]} \\ \phi_1^{[0]} \end{pmatrix}, \ \Phi_1^{[1]} = \begin{pmatrix} \varphi_1^{[1]} \\ \phi_1^{[1]} \end{pmatrix},$$
$$\Phi_1^{[2]} = \begin{pmatrix} \varphi_1^{[2]} \\ \phi_1^{[2]} \end{pmatrix}, \ldots, \tag{22}$$

where

$$\varphi_1^{[0]} = 2\sqrt{a}\mathrm{e}^{\frac{i}{2}\theta}, \quad \phi_1^{[0]} = 2\sqrt{a}\mathrm{e}^{-\frac{i}{2}\theta}, \tag{23a}$$

$$\varphi_1^{[1]} = \left(\frac{i}{8}a^{\frac{2}{3}}\left(-4x + 48it\varepsilon a^3 + 4ita - t\right)^2 \right.$$
$$\left. + \frac{i}{2}\sqrt{a}\left(-4x + 48it\varepsilon a^3 + 4ita - t\right) + \frac{\frac{i}{2}}{\sqrt{a}} \right)\mathrm{e}^{\frac{i}{2}\theta}, \tag{23b}$$

$$\phi_1^{[1]} = \left(\frac{i}{8}a^{\frac{2}{3}}\left(-4x + 48it\varepsilon a^3 + 4ita - t\right)^2 \right.$$
$$\left. - \frac{i}{2}\sqrt{a}\left(-4x + 48it\varepsilon a^3 + 4ita - t\right) + \frac{\frac{i}{2}}{\sqrt{a}} \right)\mathrm{e}^{-\frac{i}{2}\theta}. \tag{23c}$$

$\varphi_1^{[2]}$ and $\phi_1^{[2]}$ are given in the "Appendix."

Other expressions are too cumbersome to write them down. In the following discussions, we set $a = 1$ and $k = 0$ to simplify the calculation process. Then, we have $q[0] = \mathrm{e}^{i\theta}$ with $\theta = (1 + 6\varepsilon)t$ and $\lambda = -i$.

It is clearly seen that $\Phi_1^{[0]}$ is a solution of the Lax pair (3a) and (3b) at $q[0] = \mathrm{e}^{i\theta}$ and $\lambda = -i$. Hence, substituting $\Phi_1^{[0]}$, $q[0] = \mathrm{e}^{i\theta}$ and $\lambda = -i$ into Eq. (16), we obtain a trivial solution of Eq. (1)

$$q[1] = -\mathrm{e}^{i\theta}, \tag{24}$$
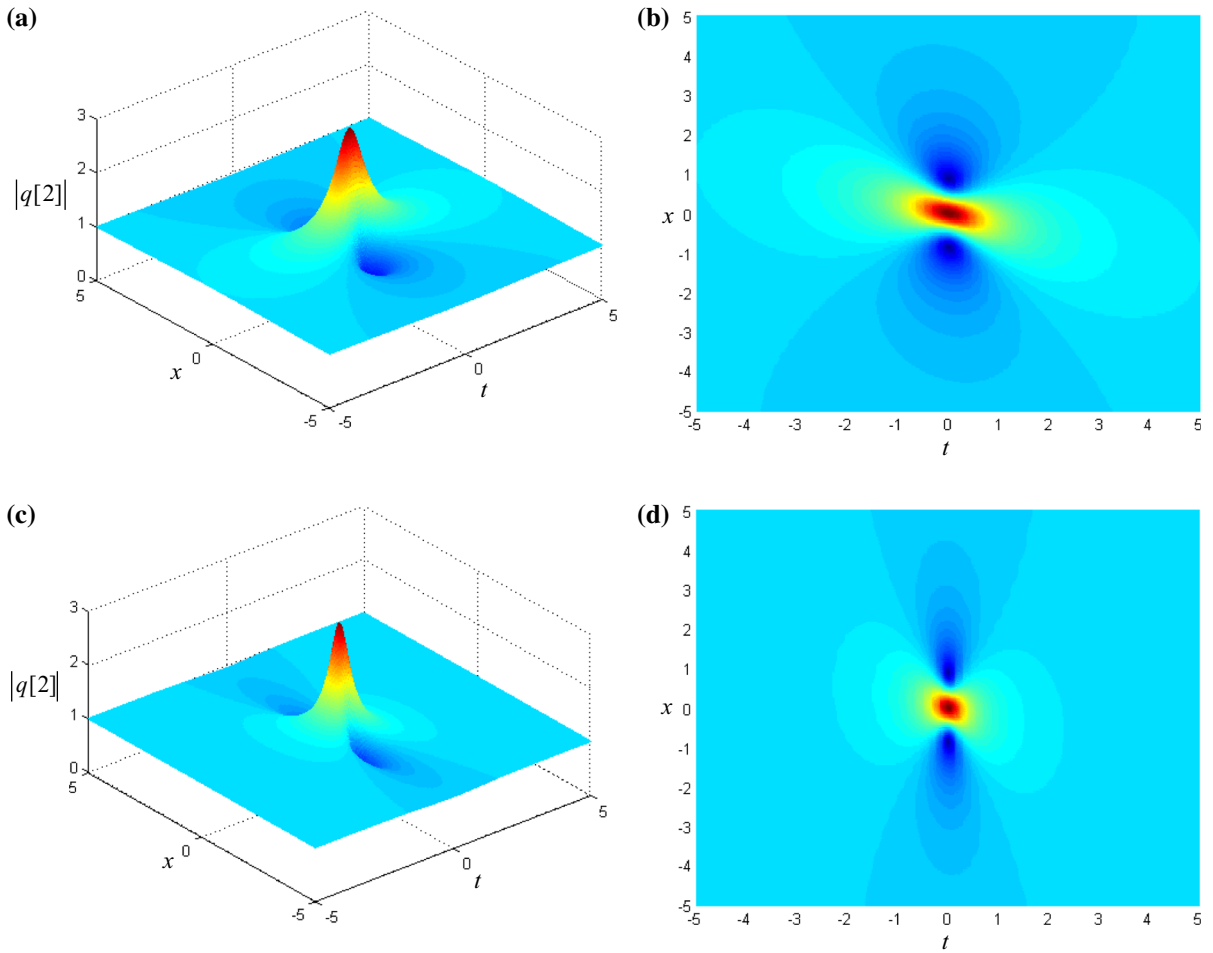
and

$$T_1[1] = \begin{pmatrix} -i & i\mathrm{e}^{i\theta} \\ i\mathrm{e}^{-i\theta} & -i \end{pmatrix}. \tag{25}$$

Consider the following limit

$$\lim_{\eta \to 0} \frac{[T_1[1]|_{\lambda = \lambda_1 + \eta}]\Psi}{\eta} = \lim_{\eta \to 0} \frac{[\eta + T_1[1]|_{\lambda = \lambda_1}]\Psi}{\eta}$$
$$= \Phi_1^{[0]} + T_1[1](\lambda_1)\Phi_1^{[1]}$$
$$= \Phi_1[1], \tag{26a}$$

$$\Phi_1[1] = \begin{pmatrix} \varphi_1[1] \\ \phi_1[1] \end{pmatrix}, \tag{26b}$$

(a)

(b)

(c)

(d)

Fig. 1 First-order rogue wave $|q[2]|$ and the density picture are plotted, **a**, **b** with parameter $\varepsilon = 0$; **c**, **d** with parameter $\varepsilon = 0.1$

where

$$\varphi_1[1] = (-4x + 48it\varepsilon + 4it - t + 2)\,\mathrm{e}^{\frac{i}{2}\theta}, \qquad (27a)$$

$$\phi_1[1] = -(-4x + 48it\varepsilon + 4it - t - 2)\,\mathrm{e}^{-\frac{i}{2}\theta}. \qquad (27b)$$

Substituting $\Phi_1^{[0]}$, $\Phi_1^{[1]}$ and $\lambda = -i$ into Eq. (16), we obtain the first-order solution of the rogue wave for Eq. (1)

and

$$T_1[2] = \begin{pmatrix} -i - \frac{4i(t+4x)}{\Delta} & \frac{i\mathrm{e}^{i\theta}\Delta_1}{\Delta} \\ \frac{i\mathrm{e}^{-i\theta}\Delta_2}{\Delta} & -i + \frac{4i(t+4x)}{\Delta} \end{pmatrix}, \qquad (29)$$

where

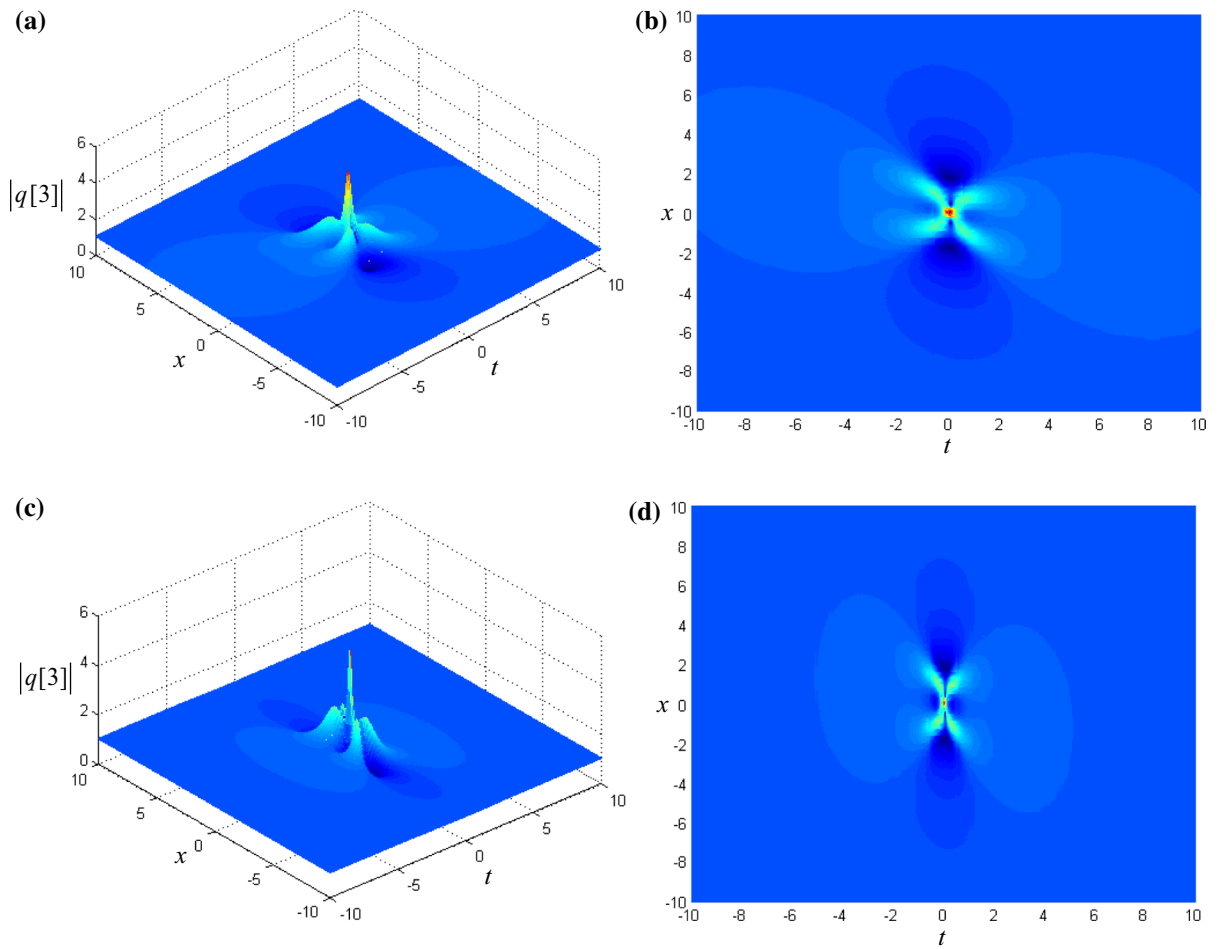$$\Delta = 4 + 2304t^2\varepsilon^2 + 384t^2\varepsilon \\ + 16x^2 + 8xt + 17t^2, \qquad (30a)$$

$$q[2] = \left(-1 - \frac{2(4 - 2304t^2\varepsilon^2 - 384t^2\varepsilon - 16x^2 - 8xt - 17t^2 + 192it\varepsilon + 16it)}{4 + 2304t^2\varepsilon^2 + 384t^2\varepsilon + 16x^2 + 8xt + 17t^2}\right)\mathrm{e}^{i\theta}, \qquad (28)$$

(a)

(b)

(c)

(d)

Fig. 2 Second-order rogue waves $|q[3]|$ and the density picture are plotted, **a**, **b** with parameters $\varepsilon = 0$ and $a_1 = b_1 = 0$; **c**, **d** with parameters $\varepsilon = 0.1$ and $a_1 = b_1 = 0$

$$\Delta_1 = 4 - 2304t^2\varepsilon^2 - 384t^2\varepsilon$$
$$\quad - 16x^2 - 8xt - 17t^2 + 192it\varepsilon + 16it, \quad (30b)$$

$$\Delta_2 = 4 - 2304t^2\varepsilon^2 - 384t^2\varepsilon$$
$$\quad - 16x^2 - 8xt - 17t^2 - 192it\varepsilon - 16it. \quad (30c)$$

Next, consider the following limit

$$\lim_{\eta \to 0} \frac{[\eta + T_1[2]|_{\lambda=\lambda_1}]\,[\eta + T_1[1]|_{\lambda=\lambda_1}]\Psi}{\eta^2}$$

$$= \Phi_1^{[0]} + (T_1[1](\lambda_1) + T_1[2](\lambda_1))\,\Phi_1^{[1]}$$

$$\quad + T_1[2](\lambda_1)T_1[1](\lambda_1)\Phi_1^{[2]} = \Phi_1[2], \quad (31a)$$

$$\Phi_1[2] = \begin{pmatrix} \varphi_1[2] \\ \phi_1[2] \end{pmatrix}, \quad (31b)$$
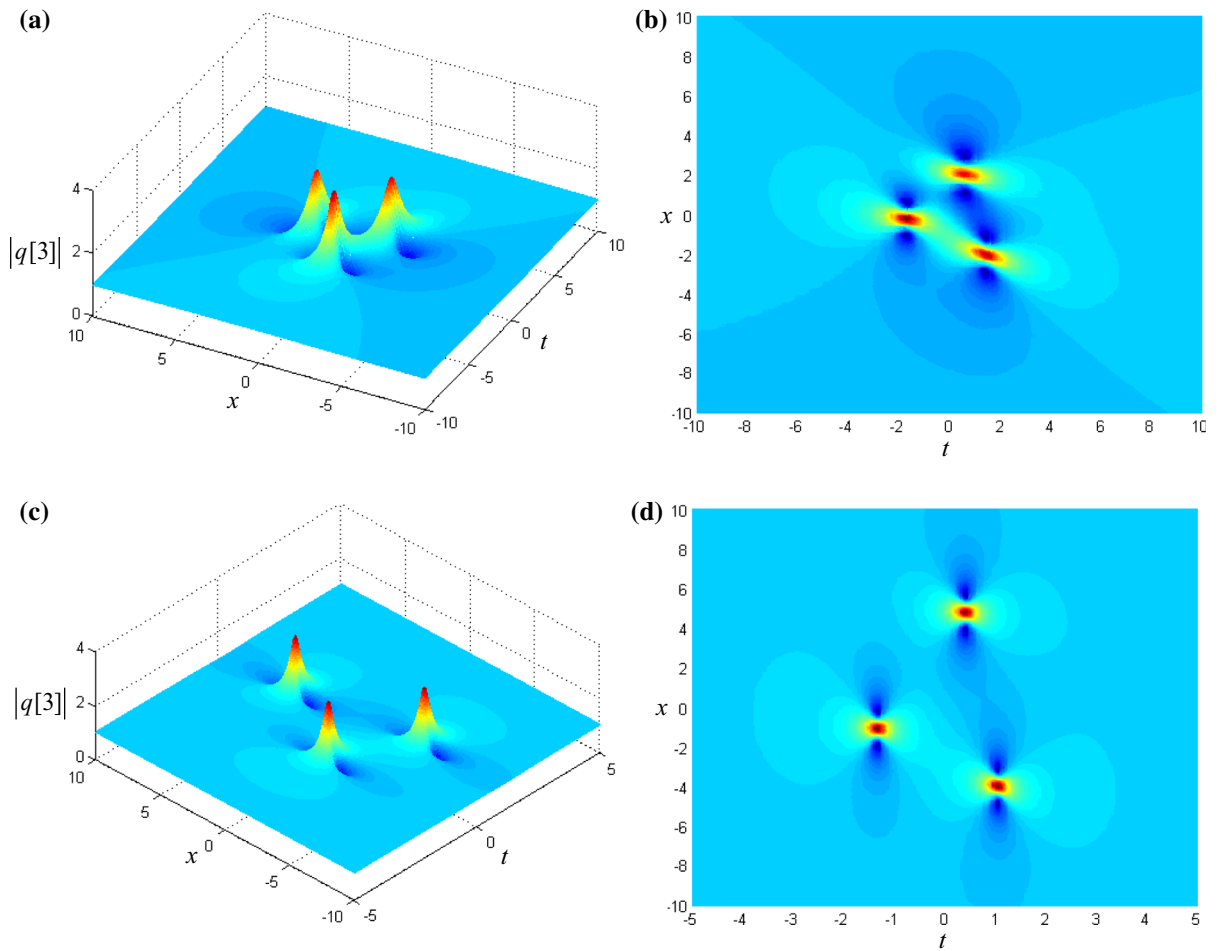
where $T_1[2]$ and $\Phi_1[2]$ can be calculated by the Maple program.

We do not give the expression of $\Phi_1[2]$ since it is rather cumbersome to write down. Substituting $\Phi_1^{[0]}$, $\Phi_1^{[1]}$, $\Phi_1^{[2]}$ and $\lambda = -i$ into Eq. (16), we obtain the second-order solution of the rogue wave for Eq. (1)

$$q[3] = q[2] - 4\frac{\varphi_1[2] \cdot \phi_1[2]^*}{|\varphi_1[2]|^2 + |\phi_1[2]|^2}. \quad (32)$$

Furthermore, we focus on the third-order solution $q[4]$ of Eq. (1). Consider the following limitation

$$\lim_{\eta \to 0} \frac{[\eta + T_1[3]|_{\lambda=\lambda_1}]\,[\eta + T_1[2]|_{\lambda=\lambda_1}]\,[\eta + T_1[1]|_{\lambda=\lambda_1}]\Psi}{\eta^3}$$

$$= \Phi_1^{[0]} + (T_1[1](\lambda_1) + T_1[2](\lambda_1) + T_1[3](\lambda_1))\,\Phi_1^{[1]}$$

$$\quad + (T_1[2](\lambda_1)T_1[1](\lambda_1) + T_1[3](\lambda_1)T_1[1](\lambda_1)$$

$$\quad + T_1[3](\lambda_1)T_1[2](\lambda_1))\Phi_1^{[2]}$$

$$\quad + T_1[3](\lambda_1)T_1[2](\lambda_1)T_1[1](\lambda_1)\Phi_1^{[3]} = \Phi_1[3], \quad (33)$$

Fig. 3 Second-order rogue waves $|q[3]|$ and the density picture are plotted, **a**, **b** with parameters $\varepsilon = 0$ and $a_1 = b_1 = 5$; **c**, **d** with parameters $\varepsilon = 0.2$ and $a_1 = b_1 = 60$

$$\Phi_1[3] = \begin{pmatrix} \varphi_1[3] \\ \phi_1[3] \end{pmatrix}, \qquad (34)$$

where $T_1[3]$ and $\Phi_1[3]$ are calculated by the Maple program.

It is also seen that the expression of $\Phi_1[3]$ is rather tedious to write them down in this paper. Substituting $\Phi_1^{[0]}, \Phi_1^{[1]}, \Phi_1^{[2]}, \Phi_1^{[3]}$ and $\lambda = -i$ into Eq. (16), we obtain the third-order rogue waves of Eq. (1)

$$q[4] = q[3] - 4 \frac{\varphi_1[3] \cdot \phi_1[3]^*}{|\varphi_1[3]|^2 + |\phi_1[3]|^2}. \qquad (35)$$

Lastly, consider the following limit

$$\lim_{\eta \to 0} \frac{[\eta + T_1[4]|_{\lambda=\lambda_1}][\eta + T_1[3]|_{\lambda=\lambda_1}][\eta + T_1[2]|_{\lambda=\lambda_1}][\eta + T_1[1]|_{\lambda=\lambda_1}]\Psi}{\eta^4}$$

$$= \Phi_1^{[0]} + (T_1[1](\lambda_1) + T_1[2](\lambda_1) + T_1[3](\lambda_1)$$
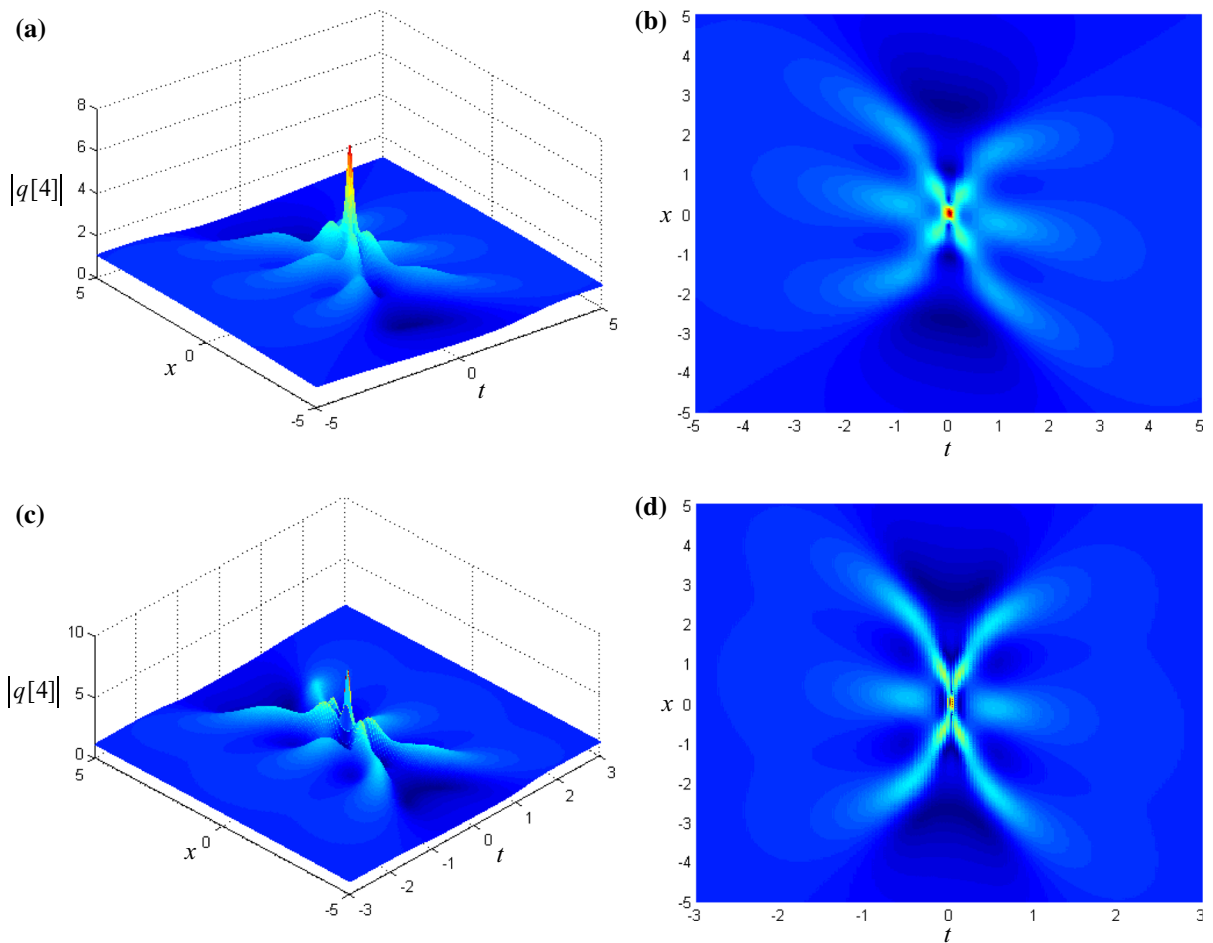
$$+ T_1[4](\lambda_1))\Phi_1^{[1]} + (T_1[2](\lambda_1)T_1[1](\lambda_1)$$

$$+ T_1[3](\lambda_1)T_1[1](\lambda_1) + T_1[4](\lambda_1)T_1[1](\lambda_1)$$

$$+ T_1[3](\lambda_1)T_1[2](\lambda_1) + T_1[4](\lambda_1)T_1[2](\lambda_1)$$

$$+ T_1[4](\lambda_1)T_1[3](\lambda_1))\Phi_1^{[2]} + (T_1[3](\lambda_1)T_1[2](\lambda_1)T_1[1](\lambda_1)$$

$$+ T_1[4](\lambda_1)T_1[3](\lambda_1)T_1[2](\lambda_1)$$

$$+ T_1[4](\lambda_1)T_1[3](\lambda_1)T_1[1](\lambda_1)$$

$$+ T_1[4](\lambda_1)T_1[2](\lambda_1)T_1[1](\lambda_1))\Phi_1^{[3]} = \Phi_1[4], \qquad (36a)$$

$$\Phi_1[4] = \begin{pmatrix} \varphi_1[4] \\ \phi_1[4] \end{pmatrix}. \qquad (36b)$$

where $T_1[4]$ and $\Phi_1[4]$ are calculated by the Maple program.

Substituting $\Phi_1^{[0]}, \Phi_1^{[1]}, \Phi_1^{[2]}, \Phi_1^{[3]}, \Phi_1^{[4]}$ and $\lambda = -i$ into Eq. (16), we obtain the fourth-order rogue waves of Eq. (1)

$$q[5] = q[4] - 4 \frac{\varphi_1[4] \cdot \phi_1[4]^*}{|\varphi_1[4]|^2 + |\phi_1[4]|^2}. \qquad (37)$$

(a)

(b)

(c)

(d)

Fig. 4 Third-order the rogue waves $|q[4]|$ and the density picture are plotted, **a**, **b** with parameters $\varepsilon = 0, a_1 = b_1 = 0$ and $a_2 = b_2 = 0$; **c**, **d** with parameters $\varepsilon = 0.1$, $a_1 = b_1 = 0$ and $a_2 = b_2 = 0$

4 Numerical results

In this section, we use numerical results to investigate the nonlinear dynamic properties of the rogue waves for the inhomogeneous higher-order nonlinear Schrödinger equation. The plot of the first-order rogue wave is depicted, as shown in Fig. 1. Figure 1a represents the amplitude in the space $(t, x, q[2])$, and Fig. 1b is the density plot in the plane (t, x). In Fig. 1a, b, we have $\varepsilon = 0$. In Fig. 1c, d, there is $\varepsilon = 0.1$. As ε increases, it is found that the temporal range for the appearance of the rogue wave shortens.

In Eq. (32), there are three free parameters ε, a_1 and b_1. We will take different values to display different second-order rogue waves. For the general case $\varepsilon = 0$ and $a_1 = b_1 = 0$, the corresponding plot of the second-

order rogue wave is depicted, as shown in Fig. 2a, b. Figure 2a is a fundamental pattern in which a single maximum appears at the center. By slightly adjusting the parameter $\varepsilon = 0.1$ and keeping other parameters constant, the rogue waves are also depicted, as shown in Fig. 2c, d. In Figure 2d, the spatial range extends a little toward both sides, but the temporal range for the appearance of the rogue wave shortens.

Then, we study the influence of the separating function $\Omega(\eta)$ on the second-order rogue wave. The plots of the second-order rogue waves are depicted, as shown in Fig. 3. In Fig. 3a, b, we have $\varepsilon = 0$ and $a_1 = b_1 = 5$. In Fig. 3a, b, the solution $q[2]$ splits into three first-order rogue waves, but are connected each other. Three first-order rogue waves have a structure of the equilateral triangle. In Fig. 3c, d, there are $\varepsilon = 0.2$ and

(a)

(b)

(c)

(d)
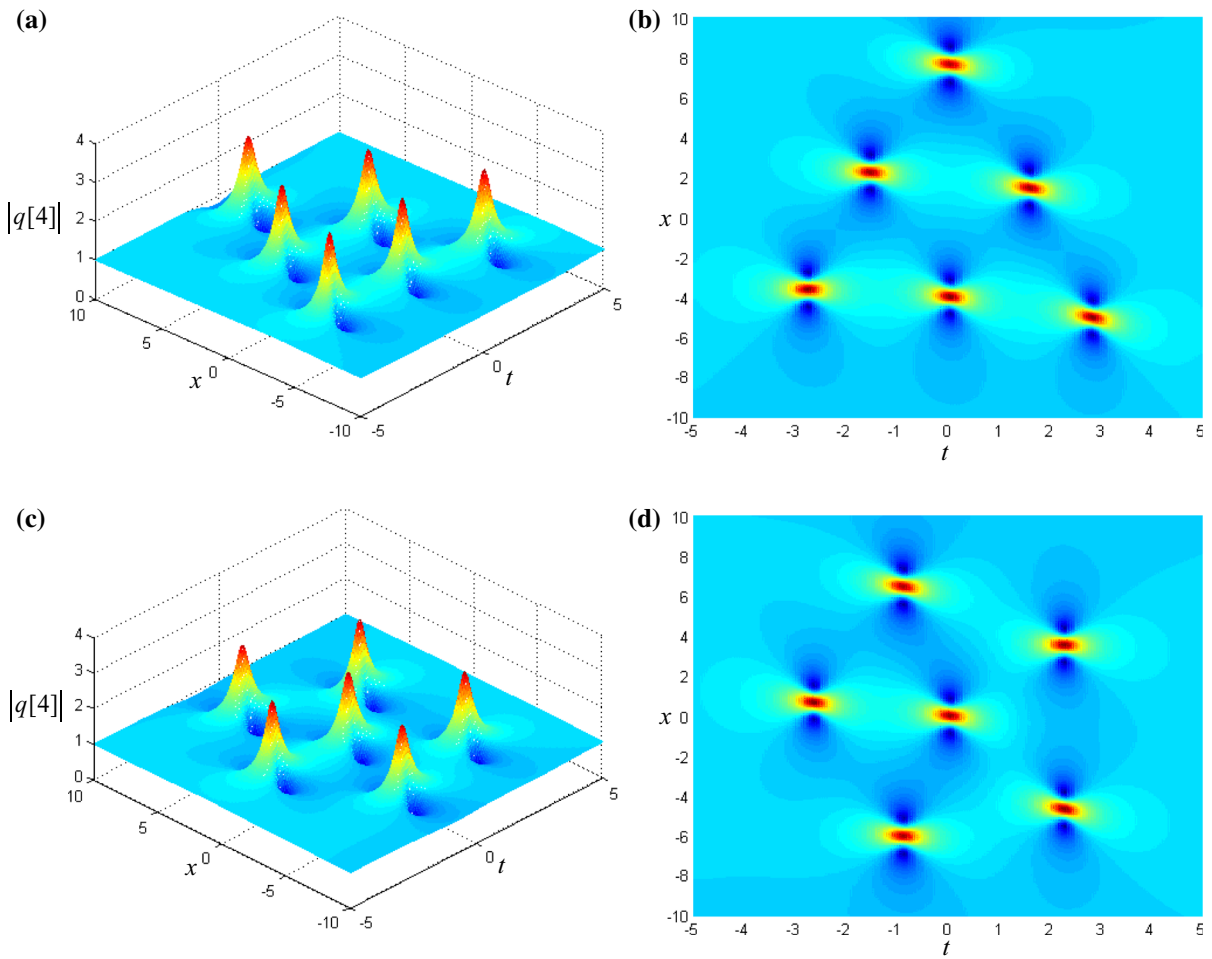
Fig. 5 Third-order rogue waves $|q[4]|$ and the density picture are plotted, **a**, **b** with parameters $\varepsilon = 0.1$ and $b_1 = 50$; **c**, **d** with parameters $\varepsilon = 0.1$ and $b_2 = 1000$

$a_1 = b_1 = 60$. The solution $q[3]$ is also composed of three first-order rogue waves and forms a structure of the triangle, but is separated completely.

There are five parameters ε, a_1, b_1, a_2 and b_2 in the third-order solution $q[4]$. The corresponding plots of this solution are depicted, as shown in Fig. 4. In Fig. 4a, b, we have $\varepsilon = 0$, $a_1 = b_1 = 0$ and $a_2 = b_2 = 0$. There is a single maximum peak at the center, and six small peaks lie around the maximum one. In this case, the maximum amplitude of $q[4]$ is 7. Changing the parameter $\varepsilon = 0.1$ and keeping other parameters same, the solution $q[4]$ is depicted, as shown in Fig. 4c, d. In this case, the temporal range for the appearance of the rogue wave shortens with the increase in the parameter ε.

When we select the parameters as $\varepsilon = 0.1$ and $b_1 = 50$, the corresponding plots of the solution $q[4]$

are depicted, as shown in Fig. 5a, b. When we only change the parameter $b_2 = 1000$, the corresponding plots of the solution $q[4]$ are given in Fig. 5c, d. Comparing Fig. 5a with 5c, it is found that the third-order rogue waves consist of six first-order rogue waves. Meanwhile, it is observed from Fig. 5b that six first-order rogue waves form an equilateral triangle. However, it is obviously seen from Fig. 5d that these waves also form a pentagon. One wave is located in the center, and other waves are put on the vertices of the pentagon.

There are seven parameters ε, a_1, b_1, a_2, b_2, a_3 and b_3 in the fourth-order solution $q[5]$. The corresponding plots of this solution are depicted, as shown in Fig. 6. In Fig. 6a, b, we have $\varepsilon = 0$, $a_1 = b_1 = 0$, $a_2 = b_2 = 0$ and $a_3 = b_3 = 0$. It is a fundamental pattern of the fourth-order rogue wave and is a single maximum at

(a)

(b)

(c)

(d)
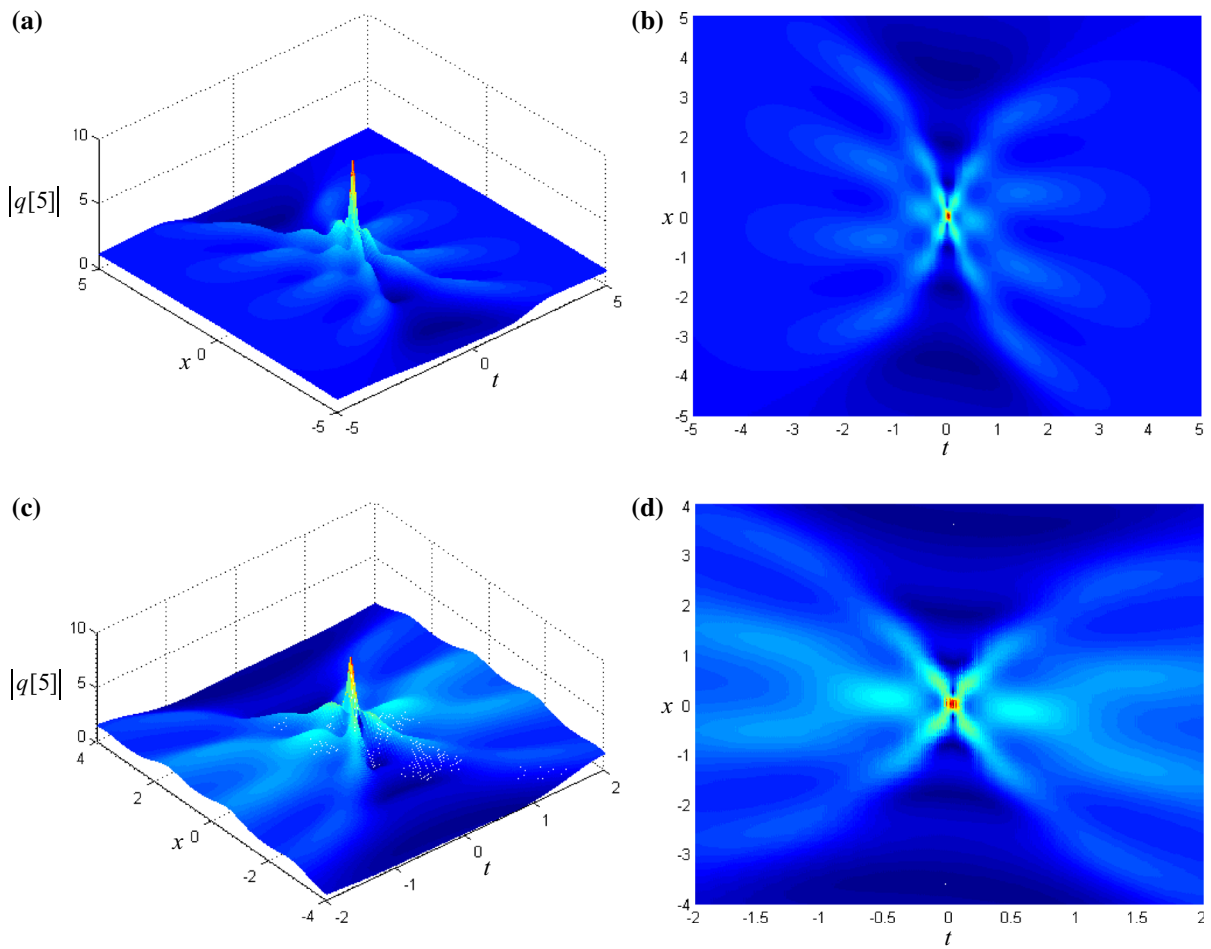
Fig. 6 Fourth-order rogue waves $|q[5]|$ and the density picture are plotted, **a**, **b** with parameters $\varepsilon = 0$, $a_1 = b_1 = 0$, $a_2 = b_2 = 0$ and $a_3 = b_3 = 0$; **c**, **d** with parameters $\varepsilon = 0.02$, $a_1 = b_1 = 0$, $a_2 = b_2 = 0$ and $a_3 = b_3 = 0$

the center, and eight small peaks lie around the maximum one. In this case, the maximum amplitude of $q[5]$ is 9. Changing the parameter $\varepsilon = 0.02$ and keeping other parameters same, the solution $q[5]$ is depicted, as shown in Fig. 6c, d. In this case, the temporal range for the appearance of the rogue wave shortens with the increase in the parameter ε.

Setting $\varepsilon = 0.02$ and $b_3 = 35,000$, the corresponding plots of the solution $q[5]$ are depicted, as shown in Fig. 7a, b. In Fig. 7a, the fourth-order rogue waves are composed of seven first-order rogue waves and one second-order rogue wave. In Fig. 7b, seven first-order rogue waves form a ring structure and the second-order rogue wave lie in the center of the ring.

With the increase in the order of the solution $q[N]$, the solutions of the rogue wave contain more free para-

meters and display more interesting spatial–temporal structures. It is guessed that these new structures could be a polygon which could be extended to the general Nth-order systems.

5 Conclusions

In this paper, the first-order to the fourth-order rogue waves are investigated using the generalized Darboux transformation for the inhomogeneous higher-order nonlinear Schrödinger equation for the first time. A brief introduction of the DT is given, and the generalized DT is studied using the Taylor series expansion of a special solution to the linear spectral problem and a limit procedure. Some different types of figures are
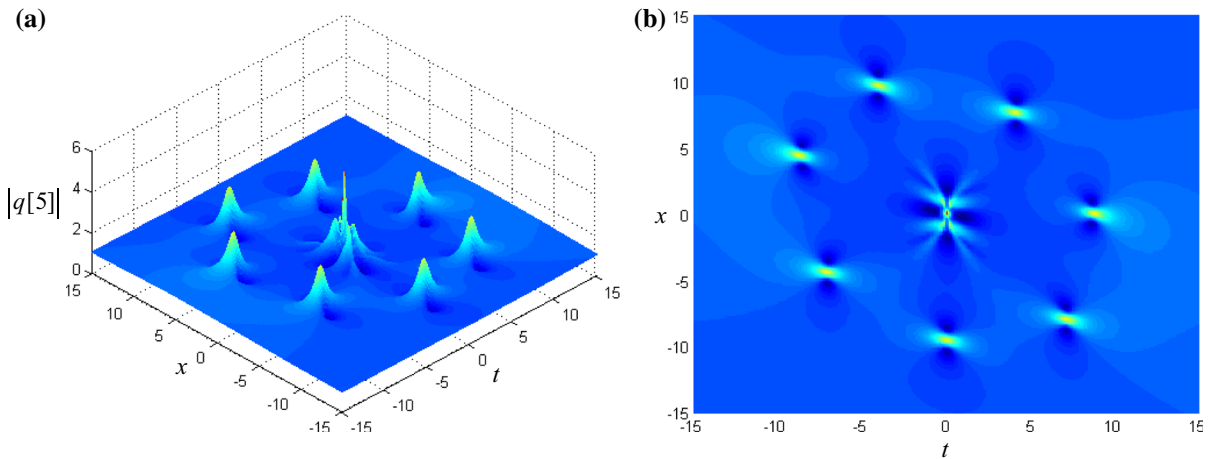
Fig. 7 Fourth-order rogue wave $|q[5]|$ and the density picture are plotted with parameters $\varepsilon = 0.02$ and $b_3 = 35{,}000$

explicitly obtained to illustrate the nonlinear dynamic properties of the rogue waves for the inhomogeneous higher-order nonlinear Schrödinger equation by changing the free parameters. Generally speaking, the Nth-order rogue waves contain $2n - 1$ free parameters and the total number of the peaks is $\frac{n(n+1)}{2}$ in terms of a complete decomposition pattern. The structures of the Nth-order rogue waves depend on the choice of the free parameters. If we continue to use the generalized DT procedure, it will be found that there exist the solutions of the more complicated rogue waves. We are looking forward to see that the theoretical results may be verified by the experiments in the future.

Appendix

Analytical expressions of the coefficients in Eq. (21) are given as

$$\varphi_1^{[2]} = \left(\frac{1}{\sqrt{a}} \left(\frac{i}{96} \left(27648a^9 t^3 \varepsilon^2 + 2304a^7 t^3 \varepsilon \right.\right.\right.$$
$$- 96a^3 xt^2 - 192a^3 x^2 t + 64a^5 t^3 - 240ta$$
$$- 12t^3 a^3 1152i a^6 t^3 \varepsilon + 27648i a^8 xt^2 \varepsilon^2$$
$$+ 4608i a^6 xt^2 \varepsilon - 1152a^5 xt^2 \varepsilon - 2304a^5 x^2 t\varepsilon$$
$$\times 110592a^{11} t^3 \varepsilon^3 + 192i a^4 xt^2 + 6912i a^8 t^3 \varepsilon^2$$

$$- 48i a^2 x^2 t - 12i a^2 xt^2 - 5952t\varepsilon a^3 - 192aa_1$$
$$- 48ix - 12it - 144a^5 t^3 \varepsilon - 192i ab_1$$
$$\left. - 64i a^2 x^3 - i a^2 t^3 + 48i a^4 t^3 \right)$$
$$- \frac{1}{32}\sqrt{a}\left(-4x + 48it\varepsilon a^3 - t + 4ita \right)^2$$
$$+ 1/16 a^{-3/2} + \frac{1}{768}\sqrt{a}\left(-4x + 48it\varepsilon a^3 \right.$$
$$- t + 4ita)\left(- 1152a^6 t^3 \varepsilon - 192a^4 xt^2 \right.$$
$$+ 192x + 48t - 48a^4 t^3 - 4608a^6 xt^2 \varepsilon$$
$$- 1152i a^5 xt^2 \varepsilon - 2304i a^5 x^2 t\varepsilon$$
$$- 27648a^8 xt^2 \varepsilon^2 + 64a^2 x^3 + a^2 t^3 - 6912a^8 t^3 \varepsilon^2$$
$$+ 48a^2 x^2 t + 12a^2 xt^2 - 960ita - 12i a^3 t^3$$
$$\times 64i a^5 t^3 - 768i aa_1 + 768ab_1 - 23808it\varepsilon a^3$$
$$- 144i a^5 t^3 \varepsilon - 96i a^3 xt^2 + 27648i a^9 t^3 \varepsilon^2$$
$$\times 2304i a^7 t^3 \varepsilon - 192i a^3 x^2 t$$
$$\left.\left.\left. + 110592i a^{11} t^3 \varepsilon^3 \right)\right)\right) e^{\frac{i}{2}\theta},$$

$$\varphi_1^{[2]} = \left(-\frac{1}{\sqrt{a}} \left(\frac{i}{96} \left(110592a^{11} t^3 \varepsilon^3 + 27648a^9 t^3 \varepsilon^2 \right.\right.\right.$$
$$+ 2304a^7 t^3 \varepsilon - 96a^3 xt^2 + 192a^3 x^2 t$$
$$+ 27648i a^8 xt^2 \varepsilon^2 - 48i a^2 x^2 t + 64a^5 t^3$$
$$- 240ta - 12t^3 a^3 + 1152i a^6 t^3 \varepsilon 12i a^2 xt^2$$
$$+ 6912i a^8 t^3 \varepsilon^2 + 192i a^4 xt^2 - 48ix - 12it$$
$$- i a^2 t^3 - 192i ab_1 + 48i a^4 t^3 - 64i a^2 x^3$$
$$- 1152a^5 xt^2 \varepsilon - 2304a^5 x^2 t\varepsilon - 192aa_1$$
$$- 5952t\varepsilon a^3 - 144a^5 t^3 \varepsilon 4608i a^6 xt^2 \varepsilon \Big)\Big)$$

$$-\frac{1}{32}\sqrt{a}\Big(-4x+48it\varepsilon a^3-t+4ita\Big)^2$$
$$+1/16a^{-3/2}+\frac{1}{768}\sqrt{a}\Big(-4x+48it\varepsilon a^3$$
$$-t+4ita\Big)\Big(-96ia^3xt^2-192ia^3x^2t$$
$$+192x+48t+64ia^5t^3+110592ia^{11}t^3\varepsilon^3$$
$$+27648ia^9t^3\varepsilon^2-768iaa_1-12ia^3t^3$$
$$-960ita+12a^2xt^2+48a^2x^2t-192a^4xt^2$$
$$+768ab_1-144ia^5t^3\varepsilon+2304ia^7t^3\varepsilon$$
$$-23808it\varepsilon a^3-4608a^6xt^2\varepsilon-27648a^8xt^2\varepsilon^2$$
$$-48a^4t^3+a^2t^3+64a^2x^3-6912a^8t^3\varepsilon^2$$
$$-1152t^3a^6\varepsilon\quad-1152ia^5xt^2\varepsilon$$
$$-2304ia^5x^2t\varepsilon\Big)\Big)e^{-\frac{i}{2}\theta}. \tag{38}$$

References

1. Müller, P., Garrett, C., Osborne, A.: Rogue waves. Oceanography **18**, 66–75 (2005)
2. Akhmediev, N., Ankiewicz, A., Taki, M.: Waves that appear from nowhere and disappear without a trace. Phys. Lett. A **373**, 675–678 (2009)
3. Solli, D.R., Ropers, C., Koonath, P., Jalali, B.: Optical rogue waves. Nature **450**, 1054–1058 (2007)
4. Bludov, Y.V., Konotop, V.V., Akhmediev, N.: Matter rogue waves. Phys. Rev. A **80**, 033610 (2009)
5. Ganshin, A.N., Efimov, V.B., Kolmakov, G.V., Mezhov-Deglin, L.P., McClintock, P.V.E.: Observation of an inverse energy cascade in developed acoustic turbulence in superfluid helium. Phys. Rev. Lett. **101**, 065303 (2008)
6. Kharif, C., Pelinovsky, E.: Physical mechanisms of the rogue wave phenomenon. Eur. J. Mech. B/Fluids **22**, 603–634 (2003)
7. Janssen, P.A.: Nonlinear four-wave interactions and freak waves. J. Phys. Oceanogr. **33**, 863–884 (2003)
8. Onorato, M., Osborne, A.R., Serio, M., et al.: Freak waves in random oceanic sea states. Phys. Rev. Lett. **86**, 5831–5834 (2001)
9. Peregrine, D.H.: Water waves, nonlinear Schrödinger equations and their solutions. J. Aust. Math. Soc. Ser. B **25**, 16–43 (1983)
10. Akhmediev, N., Ankiewicz, A., Soto-Crespo, J.M.: Rogue waves and rational solutions of the nonlinear Schrödinger equation. Phys. Rev. E **80**, 026601 (2009)
11. Zhu, H.P.: Nonlinear tunneling for controllable rogue waves in two dimensional graded-index waveguides. Nonlinear Dyn. **72**, 873–882 (2013)
12. Zakharov, V.E., Shabat, A.B.: Exact theory of two-dimensional self-focusing and one-dimensional self-modulation of waves in nonlinear media. Sov. Phys. JETP **34**, 62–69 (1971)
13. Matveev, V.B., Salle, M.A.: Darboux Transformation and Solitons. Springer, Berlin (1991)
14. Zhaqilao, : On Nth-order rogue wave solution to the generalized nonlinear Schrödinger equation. Phys. Lett. A **377**, 855–859 (2013)
15. Dai, C.Q., Zhu, H.P.: Superposed Akhmediev breather of the (3+1)-dimensional generalized nonlinear Schrödinger equation with external potentials. Ann. Phys. **341**, 142–152 (2014)
16. Yang, B., Zhang, W.G., Zhang, H.Q., Pei, S.B.: Generalized Darboux transformation and rogue wave solutions for the higher-order dispersive nonlinear Schrödinger equation. Phys. Scripta **88**, 065004 (2013)
17. Jiang, H.J., Xiang, J.J., Dai, C.Q., Wang, Y.Y.: Nonautonomous bright soliton solutions on continuous wave and cnoidal wave backgrounds in blood vessels. Nonlinear Dyn. **75**, 201–207 (2014)
18. Ling, L.M., Guo, B.L., Zhao, L.C.: High-order rogue waves in vector nonlinear Schrödinger equations. Phys. Rev. E **89**, 041201 (2014)
19. Lü, X., Peng, M.S.: Painlevé-integrability and explicit solutions of the general two-coupled nonlinear Schrödinger system in the optical fiber communications. Nonlinear Dyn. **73**, 405–410 (2013)
20. Wang, Y.Y., Dai, C.Q., Wang, X.G.: Stable localized spatial solitons in PT-symmetric potentials with power-law nonlinearity. Nonlinear Dyn. **77**, 1323–1330 (2014)
21. Dai, C.Q., Wang, X.G., Zhou, G.Q.: Stable light-bullet solutions in the harmonic and parity-time-symmetric potentials. Phys. Rev. A **89**, 013834 (2014)
22. Radha, R., Kumar, V.R.: Explode-decay solitons in the generalized inhomogeneous higher-order nonlinear Schrödinger equations. Zeitschrift fur Naturforschung A **62**, 381–386 (2007)
23. Calogero, F., Degasperis, A.: Conservation laws for classes of nonlinear evolution equations solvable by the spectral transform. Commun. Math. Phys. **63**, 155–176 (1978)
24. Lakshmanan, M., Bullough, R.K.: Geometry of generalised nonlinear Schrödinger and Heisenberg ferromagnetic spin equations with linearly x-dependent coefficients. Phys. Lett. A **80**, P287–292 (1980)
25. Abdulleav, F.: Theory of Soliton in Inhomogeneous Media. New York (1984)
26. Chen, H.H., Liu, C.S.: Nonlinear wave and soliton propagation in media with arbitrary inhomogeneities. Phys. Fluids **21**, 377–380 (1978)
27. Zhong, W.Z., Bai, Y.Q., Wu, K.: Generalized inhomogeneous Heisenberg ferromagnet model and generalized nonlinear Schrödinger equation. Phys. Lett. A **352**, 64–68 (2006)
28. Guo, B.L., Ling, L.M., Liu, Q.P.: Nonlinear Schrodinger equation: generalized Darboux transformation and rogue wave solutions. Phys. Rev. E **85**, 026607 (2012)
29. Dubard, P., Gaillard, P., Klein, C., Matveev, V.B.: On multirogue wave solutions of the NLS equation and position solutions of the KdV equation. Eur. Phys. J. Special Top. **185**, 247–258 (2010)
30. Dubard, P., Matveev, V.B.: Multi-rogue waves solutions of the focusing NLS equation and the KP-I equation. Nat. Hazards Earth Syst. Sci. **11**, 667–672 (2011)